Spin-torque-driven ballistic precessional switching with 50 ps impulses

O. J. Lee,[1,a)] D. C. Ralph,[1,2] and R. A. Buhrman[1]
[1]*Cornell University, Ithaca, New York 14853, USA*
[2]*Kavli Institute at Cornell, Ithaca, New York 14853, USA*

(Received 29 May 2011; accepted 16 August 2011; published online 7 September 2011)

We demonstrate reliable spin-torque-driven ballistic precessional switching using 50 ps current impulses in a spin-valve device that includes both in-plane and out-of-plane spin polarizers. Different threshold currents as the function of switching direction and current polarity enable the final orientation of the magnetic free layer to be steered, in accord with a macrospin analysis, by the sign of the pulse, eliminating the need for read-before-write toggle operation. The pulse amplitude windows for this deterministic operation are wider and more symmetric as a function of current polarity for shorter impulses, while inhomogeneous fringe fields from the polarizers lead to asymmetries as a function of current direction. © *2011 American Institute of Physics*. [doi:10.1063/1.3635782]

The fast reversal of a nanomagnet is of active interest because its study can enhance understanding of fundamental magnetic dynamics and because of the technological advantages that a successful high-speed non-volatile magnetic memory could provide. Several schemes[1–7] have been explored for fast nanomagnet switching, with the perhaps most scalable approach being demonstrated by recent experiments[8–11] which achieved reliable high-speed reversal of a thin film nanomagnet by using the spin torque (ST) from a spin-polarized current pulse as short as 100 ps. These experiments utilized devices in which a thin film free layer (FL) is located between an out-of-plane (OP) spin polarizer (OPP) and an in-plane (IP) analyzer/polarizer (IPP). In this configuration, the ST (τ_{OP}) generated by a strong OP-polarized current pulse incident upon the FL forces the FL moment out of plane, inducing a demagnetization field (H_{demag}) about which the FL begins to precess.[6,7] If the pulse width and amplitude are properly controlled, the result can be a rapid rotation of the moment by 180° to the reversed equilibrium position.

The simplest form of this OP-precessional reversal scheme has the potential disadvantage of being a toggle operation, in which both parallel (P) to anti-parallel (AP) and AP-to-P switching occur for either sign of current. This is in contrast to a deterministic operation in which the final state is controlled by the current polarity, as is the case for ST devices only utilizing IP polarized currents. However, previous OP-ST experiments[8–10] in which the IPP also exerted a strong ST, τ_{IP}, on the FL obtained differences in the threshold currents for switching as a function of current polarity and switching direction. This indicated that the final state in OP-ST devices may be determinable by pulse-current polarity, although with pulse widths $\geq$100 ps, only one current polarity showed a sufficiently wide window between the switching currents for P-to-AP and AP-to-P to yield reliable writes.[8]

Here, we report the achievement of reliable and deterministic spin torque ballistic precessional switching (STBPS) by using 50 ps current impulses, demonstrating that shorter and stronger pulses can enhance the influence of τ_{IP}, providing wider current windows for deterministic switching. Based on micromagnetic simulations, we also conclude that inhomogeneous stray magnetic fields from the two polarizers induce asymmetries in the deterministic switching windows for the two current polarities.

We fabricated nanopillar spin valve devices from thin-film multilayers with the structure: bottom lead/OPP/Cu(6)/Py(5)/Cu(12)/Py(20)/top lead (thicknesses in nm), where Py is $Ni_{80}Fe_{20}$. The OPP was Pt(10)/[Co(0.44)/Pt(0.68)]$_4$/Co(0.66)/Cu(0.3)/Co(0.66). The 5 nm Py layer served as the magnetic FL and the 20 nm Py layer was the IPP. The devices were fabricated into approximately elliptical cross-sections with dimensions 50×170 nm^2, with the etch producing slightly tapered side walls (20-30° from vertical).[12] The thickness of the IPP (20 nm) was chosen to be much greater than the spin-diffusion length (~5 nm) to ensure a strong τ_{IP}. For pulses longer than 200 ps, these devices exhibited precessional switching characteristics similar to previous meausurements[8]. Here, we focus on results obtained with 50 and 100 ps impulses.

We generated 50 ps current impulses (Fig. 1(b)) by differentiating a sharply falling step pulse, while pulses with 100 ps widths were generated with a commercial pulse generator. The current through the device was calculated taking into account the impedance mismatch between the load resistance and the 50Ω transmission line.[13] All measurements were performed at room temperature under an applied magnetic field canceling the average in-plane dipole field from the IPP. Ten devices were studied in detail and similar behavior was obtained in all cases. We define positive current to correspond to electron flow from the OPP to the FL (and to the IPP).

Figures 1(c) and 1(d) show switching probabilities (P_s) obtained from one device as a function of current amplitude, polarity, and switching direction (P-to-AP or AP-to-P) using both 50 ps and 100 ps current impulses. For the 50 ps case, reliable P-to-AP switching ($P_s \geq 95\%$) was achieved for current pulse amplitudes beyond $I^{+}_{r,P-AP} \sim 11$ mA, but AP-to-P switching was not observed up to the highest pulse level employed, from which we conclude that the threshold current ($P_s \geq 5\%$) to initiate switching is $I^{+}_{th,AP-P} > 17$ mA. This yields a deterministic window at positive pulse

a)Author to whom correspondence should be addressed. Electronic mail: ol29@cornell.edu.

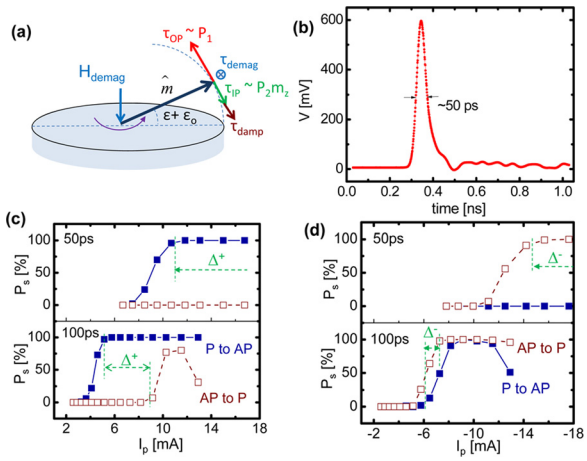

FIG. 1. (Color online) (a) Scheme of STBPS. In the case shown, the current polarity and orientations of the fixed layers are such that the OP torque promotes upward (positive z) displacement of $\hat{m}$ and the IP torque retards it. (b) Measured waveform of the ~50 ps (FWHM) current impulse injected into the device. Measured switching probabilities (P_s) using (c) positive and (d) negative 50 ps or 100 ps current impulses.

amplitudes for ST switching to the AP state of $\Delta^+(50\ \text{ps}) \equiv I^+_{th,AP-P} - I^+_{r,P-AP} > 6$ mA (Fig. 1(c)), while $\Delta^+(100\,\text{ps}) \sim 4$ mA (Fig. 1(c)). For negative 50 ps impulses, the pulse amplitude required for reliable AP-to-P switching was larger in magnitude, $I^-_{r,AP-P} \sim -15$ mA, resulting in a window $\Delta^-(50\ \text{ps}) \equiv -(I^-_{th,P-AP} - I^-_{r,AP-P}) > 3$ mA (Fig. 1(d)), while $\Delta^-(100\,\text{ps})$ was negligible. The increase in the switching windows Δ^+ and Δ^- with the reduction of pulse width to 50 ps demonstrates the possibility of implementing ultra-fast *deterministic* STBPS.

Certain aspects of the switching behavior, including the origin of the deterministic switching windows, can be understood with a simple zero-temperature (T = 0) macrospin model that utilizes the Landau-Lifshitz-Gilbert (*LLG*) equation including the effects of ST[14–16] from the two spin polarizers

$$\frac{d\hat{m}}{dt} = -\gamma\hat{m}\times\vec{H}_{eff} + \alpha\hat{m}\times\frac{d\hat{m}}{dt} + \gamma a_1(\theta_1)\hat{m}\times\hat{p}_1\times\hat{m} - \gamma a_2(\theta_2)\hat{m}\times\hat{p}_2\times\hat{m}, \quad (1)$$

where $a_i(\theta) = \frac{\hbar}{2e}\frac{I_p(t)}{\mu_o M_o V}P_i\eta_i(\theta)$ and $\vec{H}_{eff} = (H_k m_x + H_{dx} + H_a)\hat{x} + (H_{dz} - 4\pi M_o m_z)\hat{z}$. Here, γ is the gyromagnetic ratio, $\hat{m}$ is the unit vector of the FL, H_k is the anisotropy field of the FL, H_{dx} and H_{dz} are the IP and OP components of the effective dipole field H_d acting on the FL, H_a is the external applied field along the FL easy axis, $\hat{p}_1$ is the spin polarization axis of the OPP ($\hat{z}$) and $\hat{p}_2$ is of the IPP ($-\hat{x}$), $\eta(\theta) = 2\Lambda^2/[(\Lambda^2+1) + (\Lambda^2-1)\cos\theta]$, $\theta_{1(2)}$ is the angle between the FL and OPP (IPP), Λ is a torque asymmetry parameter due to spin accumulation effects (we assume symmetric electrodes), M_o is the saturation magnetization of the FL, and P_i is the spin polarization.[17]

In the STBPS, the reversals are mostly governed by the initial out-of-plane rotation angle generated by the current pulse because this angle determines the strength of H_{demag}. From Eq. (1), we have the initial equation of motion for the out-of-plane rotation

$$\frac{1+\alpha^2}{\gamma}\frac{d\varepsilon}{dt} = (a_1 + a_2\varepsilon_o) + (a_2 - \alpha\cdot 4\pi M_o)\varepsilon, \quad (2)$$

where ε is the out-of-plane offset angle of the FL moment relative to the equilibrium angle ($\varepsilon_o = H_{dz}/4\pi M_o$). The rotation angle $\varepsilon(\tau_p)$ when the pulse is terminated is $a_1(e^{(a_2-\alpha\cdot 4\pi M_o)\tau_p} - 1)/(a_2 - \alpha\cdot 4\pi M_o)$, assuming that a square pulse with the width $\tau_p = \gamma t_p/(1+\alpha^2) \approx \gamma t_p$ is applied and $\varepsilon_o = 0$. In the absence of an IPP ($a_2 = 0$), the current required to achieve a given out-of-plane rotation angle is independent of both current polarity and switching direction. However, in the presence of an IPP, as τ_{OP} forces the FL out of plane, the IPP causes an additional non-zero torque perpendicular to the sample plane, $\tau_{IP} \propto (\hat{m}\times\hat{p}_2\times\hat{m})_Z$ (see Fig. 1(a)), that, assuming the $a_1 > 0$ case, either accelerates ($a_2 > 0$) or retards ($a_2 < 0$) the out-of-plane rotation of the FL moment driven by τ_{OP}. This additional torque $(\tau_{IP})_Z$ causes a difference between the currents required for AP-to-P and P-to-AP switching for a given pulse polarity (compare Fig. 1). From Eq. (2) and using parameters appropriate to our devices (see below), the macrospin calculation yields $\Delta^+ = \Delta^- \sim 1.5$ mA, 2.5 mA, and 4.5 mA for $t_p = 200$ ps, 100 ps, and 50 ps, respectively.

Our devices have the interesting features that the P-to-AP switching current at positive bias is always less than the magnitude of the AP-to-P switching current at negative bias (τ_{IP} is favorable to the switching direction in both cases) and that the deterministic window for the positive current pulses is invariably larger than for the negative. To understand these features and the details of the STBPS, we performed T = 0 micromagnetic simulations that utilized Eq. (1) and employed the following magnetic parameters: $M_o(\text{IPP}) = 850$ emu/cm^3, $M_o(\text{FL}) = 650$ emu/cm^3, $M_o(\text{OPP}) = 870$ emu/cm^3, exchange constants $A(\text{IPP}) = A(\text{FL}) = 13\times10^{-6}$ erg, $A(\text{OPP}) = 26\times10^{-6}$ erg, OPP anisotropy $K^{\perp}(OPP) = 8\times10^6$ erg/cm^3, and FL damping $\alpha = 0.03$.[18] The simulated nano-pillar had an elliptical cross-section of 50×170 nm^2 and the mesh size was $5\times5\times2.5$ nm^3. The static magnetic configurations were first calculated by the energy minimization method[19] for an external magnetic field located at the center of the minor loop for the P and AP states. Then a current impulse ($I_p(t)$) was applied at time $t = 0$ taking into account nonzero rise and fall times, with the calculated ST exerted on the interface cells of each magnetic layer.

The micromagnetic ST simulations reveal that the STBPS in this device structure is initiated by reversal at one end of the FL ellipse, with the remainder of the FL following.[20] Fig. 2 shows the simulated time-traces of $\langle m_x\rangle$ (Figs. 2(a) and 2(b)) and $\langle m_z\rangle$ (Figs. 2(c) and 2(d)) for the left 60 nm and the right 60 nm of the FL for positive (Figs. 2(a) and 2(c)) and negative (Figs. 2(b) and 2(d)) 50 ps impulses. In this simulation, $\Lambda = 1.5$, $P_1 = 0.20$, and $P_2 = 0.37$. For both current polarities, and even for $P_2 = 0.0$, the FL reversal is an inhomogeneous process in which the right (left) side rotates faster for P-to-AP (AP-to-P) reversal, rather than the uniform rotation of a macrospin.[7]

This nonuniform reversal occurs because the reference layers' dipole fields are inhomogeneous at the position of the FL (H_{dx} is plotted in Fig. 2(a) inset) and the local critical current density J_c for OP ST excited precession depends on this

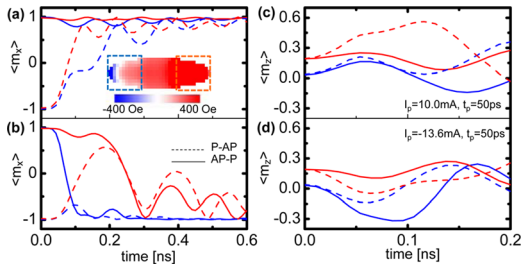

FIG. 2. (Color online) (a) Micromagnetic simulation of the time trace of $\langle m_x \rangle$ at the two ends (blue, as averaged over the left 60 nm of the FL, and red, averaged over right 60 nm (see inset)) of the FL for AP ($\langle m_x \rangle \approx 1$) and P ($\langle m_x \rangle \approx -1$) initial configurations using a positive impulse $I_p = +10$ mA, $t_p = 50$ ps (FWHM). Dashed lines: initial P configuration, solid lines: initially AP. Inset: the calculated easy-axis component of the inhomogeneous dipole fields acting on the FL. (b) Simulated time trace of $\langle m_x \rangle$ for AP and P initial configurations using a negative impulse $I_p = -13.6$ mA and $t_p = 50$ ps. (c) and (d) Simulated time trace of $\langle m_z \rangle$ for the same conditions as (a) and (b), respectively; note different time scale for (c) and (d).

field, $J_c \propto H_{k,x}^{eff} = |\pm H_k/2 + H_a + H_{dx}|$ (Ref. 21; + corresponds to AP-to-P, − to P-to-AP). For the simulated device in the AP configuration, $H_{k,L}^{eff} \approx 230$ Oe when averaged over the leftmost 60 nm of the FL, while $H_{k,R}^{eff} \approx 460$ Oe for the rightmost 60 nm. For the P configuration, the variation in H_k^{eff} is even greater, with $H_{k,L}^{eff} \approx 490$ Oe and $H_{k,R}^{eff} \approx 140$ Oe. Furthermore, H_{dZ} causes the magnetization of the FL to tilt out of plane, with this effect being stronger (weaker) on the right (left) end of the FL due to the additive (subtractive) combination of the IPP and OPP fields. The effect of H_{dZ} for $+I$ is to increase the influence of the τ_{IP} due to the significant equilibrium $\langle m_z \rangle$ ($\varepsilon_o > 0$) on the right side of the FL (Fig. 2(c) and Eq. (2)) for P-to-AP (τ_{IP} is favorable to this direction) but $\varepsilon_o \approx 0$ on the left side for AP-to-P. For $-I$, the effect of H_{dZ} provides a ε_o that is opposite to the displacement driven by the OP-ST, resulting in a smaller maximum value of $\langle m_z \rangle$ for a given pulse amplitude and hence a reduction in the influence of τ_{IP}.

The consequences of the influence of the τ_{IP} within the micromagnetic simulations can be seen in Fig. 3 which compares the $P_2 = 0.37$ and $P_2 = 0.0$ cases, and the consequences of the nonuniform dipole fields can be seen by comparing Figs. 3(a)–3(d) (w/H_d) to Figs. 3(e) and 3(f) (w/o H_d). Without H_d, we obtain, as in the original macrospin model, more uniform FL reversals and large and symmetric values for Δ^- and Δ^+, with only a small difference between $|I_{th,AP-AP}^{+}|$ and $|I_{th,AP-P}^{-}|$ arising from our use of $\Lambda = 1.5$ (Figs. 3(e) and 3(f)). With H_d, we find that for 50 ps pulses $|I_{th,P-AP}^{+}|$ is reduced while $|I_{th,AP-P}^{-}|$ is increased and $\Delta^+ > \Delta^-$. For 100 ps pulses (Fig. 3(c) and 3(d)), the simulations show that both Δ^- and Δ^+ are reduced further relative to the 50 ps case (the reduction in Δ^+ is not visible in Fig. 3 because $I_{th,AP-P}^{+}$ (100 ps) > 18 mA). This is consistent with the experiment and Eq. (2).

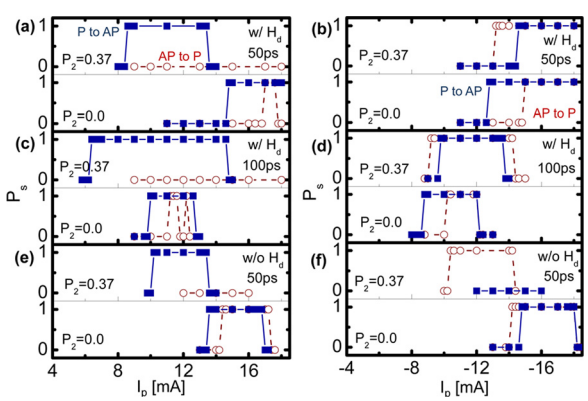

FIG. 3. (Color online) Simulated switching probabilities P_s at zero temperature. Top figures: $P_1 = 0.2$ and $P_2 = 0.37$, bottom figures: $P_1 = 0.2$ and $P_2 = 0.0$, i.e., no spin-torque from the in-plane polarizer/analyzer. Rectangles: P-to-AP switching, circles: AP-to-P. (a) and (b) P_s for 50 ps I_p impulses for (a) positive and (b) negative pulses. (c) and (d) P_s for 100 ps impulses. (e) and (f) P_s for 50 ps impulses assuming zero dipole field from the polarizer layers acting on the FL.

In summary, we have demonstrated reliable and deterministic STBPS with a 50 ps spin polarized impulse current where the shorter current impulse enhances the deterministic write operation. If the fringe fields can be reduced close to zero, then nearly symmetric deterministic windows should be achievable for both pulse polarities, enabling very fast, energy efficient STBPS.

This research was supported by the Office of Naval Research and by the NSF/NSEC program through the Cornell Center for Nanoscale Systems. We also acknowledge NSF support through use of the Cornell Nanofabrication Facility/NNIN and the Cornell Center for Materials Research facilities.

[1] J. A. Katine and E. E. Fullerton, J. Magn. Magn. Mater. **320**, 1217 (2008).
[2] H. W. Schumacher, C. Chappert, P. Crozat, R. C. Sousa, P. P. Freitas, J. Miltat, J. Fassbender, and B. Hillebrands, Phys. Rev. Lett. **90**, 017201 (2003).
[3] K. Vahaplar, A. M. Kalashnikova, A. V. Kimel, D. Hinzke, U. Nowak, R. Chantrell, A. Tsukamoto, A. Itoh, A. Kirilyuk, and Th. Rasing, Phys. Rev. Lett. **103**, 117201 (2009).
[4] S. Garzon, L. Ye, R. A. Webb, T. M. Crawford, M. Covington, and S. Kaka, Phys. Rev. B **78**, 180401(R) (2008).
[5] R. H. Koch, J. A. Katine, and J. Z. Sun, Phys. Rev. Lett. **92**, 088302 (2004).
[6] A. D. Kent, B. Özyilmaz, and E. del Barco, Appl. Phys. Lett. **84**, 3897 (2004).
[7] K. J. Lee, O. Redon, and B. Dieny, Appl. Phys. Lett. **86**, 022505 (2005).
[8] O. J. Lee, V. S. Pribiag, P. M. Braganca, P. G. Gowtham, D. C. Ralph, and R. A. Buhrman, Appl. Phys. Lett. **95**, 012506 (2009).
[9] C. Papusoi, B. Delat, B. Rodmacq, D. Houssameddine, J.-P. Michel, U. Ebels, R. C. Sousa, L. Buda-Prejbeanu, and B. Dieny, Appl. Phys. Lett. **95**, 072506 (2009).
[10] H. Liu, D. Bedau, D. Backes, J. A. Katine, J. Langer, and A. D. Kent, Appl. Phys. Lett. **97**, 242510 (2010).
[11] G. E. Rowlands, T. Rahman, J. A. Katine, J. Langer, A. Lyle, H. Zhao, J. G. Alzate, A. A. Kovalev, Y. Tserkovnyak, Z. M. Zeng, H. W. Jiang, K. Galatsis, Y. M. Huai, P. Khalili Amiri, K. L. Wang, I. N. Krivorotov, and J.-P. Wang, Appl. Phys. Lett. **98**, 102509 (2011).
[12] P. M. Braganca, O. Ozatay, A. G. F. Garcia, O. J. Lee, D. C. Ralph, and R. A. Buhrman, Phys. Rev. B **77**, 144423 (2008).
[13] S. Kaka, M. R. Pufall, W. H. Rippard, T. J. Silva, S. E. Russek, J. A. Katine, and M. Carey, J. Magn. Magn. Mater. **286**, 375 (2005).
[14] J. C. Slonczewski, J. Magn. Magn. Mater. **247**, 324 (2002).
[15] D. C. Ralph and M. D. Stiles, J. Magn. Magn. Mater. **320**, 1190 (2008).
[16] J. Xiao, A. Zangwill, and M. D. Stiles, Phys. Rev. B **72**, 014446 (2005).
[17] The field-like spin torque (J. C. Slonszewski, Phys. Rev. B **71**, 024411 (2005)) is not included here as it is negligible in spin valve devices.
[18] I. N. Krivorotov, N. C. Emley, J. C. Sankey, S. I. Kiselev, D. C. Ralph, and R. A. Buhrman, Science **307**, 228 (2005).
[19] M. J. Donahue and D. G. Porter, OOMMF User's Guide, Version 1.0, National Institute of Standards and Technology Technical Report No. NISTIR 6376 1999.
[20] See supplementary material at http://dx.doi.org/10.1063/1.3635782 for movies of the micromagnetic simulation results.
[21] D. Houssameddine, U. Ebels, B. Delaët, B. Rodmacq, I. Firastrau, F. Ponthenier, M. Brunet, C. Thirion, J.-P. Michel, L. Prejbeanu-Buda, M.-C. Cyrille, O. Redon, and B. Dieny, Nature Mater. **6**, 447 (2007).